Lithium Battery SOH Estimation: A Novel Octave and LSTM Hybrid Neural Network Approach

1st Seyed Mohammadreza Mousavi
Faculty of computer engineering and information technology
Sadjad University
Mashhad, Iran
mo.mousavi271@sadjad.ac.ir

2nd Amirhossein Rahimian Zarif
Faculty of Electrical and Biomedical Engineering
Sadjad University
Mashhad, Iran
am.rahimian578@sadjad.ac.ir

3rd Javad Hamidzadeh
Faculty of computer engineering and information technology
Sadjad University
Mashhad, Iran
j_hamidzadeh@sadjad.ac.ir

***Abstract*—The lithium battery (LIB) has emerged as a prominent area of research in energy and industrial applications, due to its superior energy density and efficient energy delivery capabilities. This study addresses the critical requirement for accurate State of Health (SOH) estimation as a significant challenge. The primary objective of this study is to utilize key battery health characteristic parameters to improve the accuracy and computational speed of SOH. Significant gaps have been identified in recent methodologies, particularly in terms of SOH estimation accuracy, computational speed, and simulation parameters. To address these limitations, a novel hybrid neural network (NN) approach is proposed, integrating octave convolution (OCT) and long short-term memory (LSTM). To demonstrate the effectiveness of the proposed method in the optimization process, a comparative analysis is conducted against Convolutional Neural Networks (CNN), OCT, LSTM, and CNN-LSTM architectures. The results indicate a significant reduction in the mean squared error (MSE), decreasing from 80.21 percent in CNN to 0.0758 percent in the proposed OCT-LSTM model. Furthermore, the root mean square error (RMSE) exhibits a substantial reduction of 64.91 percent and 58.14 percent compared to the LSTM and CNN-LSTM models, respectively. The simulation parameters used in this study were reduced from 41,228 for the CNN-LSTM model to 38,668 for the OCT-LSTM model. Empirical results show that the proposed method outperforms state-of-the-art methods in the number of parameters, MSE, RMSE, and estimation accuracy. These findings highlight the method's enhanced efficiency, computational speed, and precision, emphasizing its potential as a significant advancement in this domain.**

Keywords*—state of health (SOH) estimation, lithium battery, capacity estimation, convolutional neural networks (CNNs), long short-term memory (LSTM)

I. INTRODUCTION

Rechargeable lithium-ion batteries (LIBs) stand as vital components in applications such as portable electronics, medical devices, renewable energy storage, power grids, and electric vehicles. Known for their reliability, high energy storage capacity, long lifespan, and low self-discharge, LIBs are a globally preferred solution for energy storage and utilization [1]–[5]. The state of health (SOH), a critical parameter reflecting battery lifetime, directly influences performance under varying conditions [6], [7]. Accurate SOH estimation is critical for evaluating the degradation and safety of LIBs. Achieving high precision and reliability is essential, as battery impedance and capacity are closely tied to SOH. Increased impedance can degrade system performance, underscoring the need for precise SOH evaluation to mitigate adverse effects. However, direct SOH measurement is challenging due to its dependence on multiple factors, including the state of charge (SOC), which represents the battery storage capacity. Fortunately, accurate SOH estimation can be achieved through various methods. Research in SOH and Remaining Useful Life (RUL) prediction is broadly categorized into model-based and data-driven approaches [8], [9]. Model-based methods estimate battery capacity using the negative linear relationship between capacity and internal impedance [10], [11].

Data-driven methods are increasingly gaining attention for addressing model-based limitations, utilizing advanced machine-learning techniques to achieve their objectives [12]–[14]. The research [15] introduces the GBLS Booster; a model designed for joint SOH and RUL prediction. The model uses a CNN-Transformers-based Booster, optimized using the Tree-structured Parzen Estimator (TPE) algorithm. They also used the random forest method to refine the input data. In the article [16] they used a neural network called CNN-BiGRU, to estimate the SOH of lithium-ion batteries. They leverage voltage distribution and capacity changes from battery discharge curves to capture temporal dependencies and correlations in the data. The paper [17] focuses on parasitic side reactions at the negative electrode during charging. Comparison between LSTM and recurrent neural network (RNN) structures highlights LSTM's suitability for long-time sequence prediction. In article [18] a joint SOH-SOC estimation model based on the GWO-BP neural network was proposed. This model incorporates SOH estimation via the GWO-BP neural network, integrating it into the Ah method to correct battery capacity and enhance estimation accuracy. The [19] presents ES-EDM-DCM, which integrates the ES-EDM empirical model with a feature-driven model. Based on support vector regression, the feature-driven model is optimized using a single health feature extracted from partial battery data. The [20] focuses on battery capacity as an indicator of SOH. Furthermore, they constructed an LSTM to analyze capacity degradation patterns from a time series perspective. Studies [21]–[23] did not consider the SOH of energy storage systems (ESSs). The proposed method addresses this gap, leading to improved efficiency and performance of such systems.

This study proposes a novel model for predicting and studying the SOH of LIBs by integrating a unique methodology that combines Octave-CNN and LSTM architectures. The proposed method employs a multi-channel input structure, utilizing voltage, current, internal impedance, and temperature data to capture the intrinsic characteristics of battery aging. Unlike model-based approaches, this technique does not require prior knowledge of electrochemical principles, making it simpler to implement,

979-8-3503-6132-2/24/$31.00

computationally efficient, and less complex. The novelty of the method is the ability to enhance SOH estimation accuracy by incorporating LIBs data, yielding improved results as evidenced by lower Mean Squared Error (MSE), Mean Absolute Error (MAE), and Root Mean Squared Error (RMSE) values. Additionally, the method significantly reduces the number of parameters, resulting in faster processing speeds. The proposed approach is validated using the NASA dataset, with estimation errors and capacity differences per cycle serving as key performance metrics.

The paper is organized as follows: In Section II, the proposed method pertinent to Octave-LSTM is assessed and presented. In Section III, the related battery dataset and SOH estimation procedure are completely discussed. Section IV presents the experiment results along with learning methodologies and comparisons. Finally, Section V provides the conclusion.

II. PROPOSED METHOD

A. Data-driven models

Accurate SOH estimation depends on data-driven models that leverage extensive battery data to predict RUL. This section outlines the OCT-LSTM SOH estimation method, including preprocessing, training, and battery health estimation. Outliers are removed, and data is normalized before splitting into training, validation, and testing sets, with inputs including voltage, current, temperature, capacity, and internal impedance. Performance is evaluated by comparing results across stages. The Octave Convolution method replaces traditional convolution, reducing parameters and outperforming state-of-the-art approaches.

B. Octave convolution

Octave Convolution networks replace conventional convolution layers due to reduced spatial complexity and computational demand in CNNs. They enhance feature detection efficiency and information learning by expanding the receptive field and optimizing performance across various domains such as time-series analysis, medical imaging, remote sensing, image compression, and spectral image classification. The proposed architecture is designed to enhance data processing efficiency, utilizing octave convolution to capture both high-frequency and low-frequency components, followed by temporal feature extraction using LSTM layers. The parameter X is the input tensor of shape (B, T, F, C), where B, T, F, and C are the batch size, time dimension, feature dimension, and channel dimension=1, respectively; as (1).

$$X \in R^{B \times T \times F \times C} \tag{1}$$

The first layer is an Octave Convolutional layer, which decomposes the input into high-frequency and low-frequency components. This layer uses a kernel size of (4, 1) and 40 filters, with an octave parameter set to 1 and an output ratio of 0.5 for the low-frequency components. The input is decomposed to be prepared for the Oct convolution. The input tensor X is decomposed into high and low-frequency components using octave convolution. This decomposition process can be mathematically described as (2) and (3):

$$\begin{aligned} &X_H = X \\ &Shape: (B, T, F, 1) \end{aligned} \tag{2}$$

$$\begin{aligned} &X_L = \downarrow 2(x) \\ &shape(B, \frac{T}{2}, \frac{F}{2}, 1) \end{aligned} \tag{3}$$

Where X_H retains the high-frequency components and X_L represents the low-frequency components, obtained by down-sampling X. Here, the shape of X_H is (B, T, F, 1) and the shape of X_L is (B, T/2, F/2, 1). A series of convolutional operations are applied to extract pertinent features from both high and low frequencies. High-to-high convolution is shown as (4):

$$\begin{aligned} &Y_H^{HH} = W_{HH} * X_H \\ &Shape(B, T, F, filters) \end{aligned} \tag{4}$$

Where W_{HH} is the convolutional weight matrix for the high-to-high frequency path, and * denotes the convolution operation. The shape of Y_H^{HH} is (B, T, F, filters). High-to-low convolution known as (5):

$$\begin{aligned} &Y_L^{HL} = \downarrow 2(W_{HL} * X_H) \\ &shape(B, \frac{T}{2}, \frac{F}{2}, filters) \end{aligned} \tag{5}$$

Where W_{HL} is the convolutional weight matrix for the high-to-low frequency path, the resulting Y_L^{HL} has the shape (B, T/2, F/2, filters). The sign $\downarrow$ denotes the down-sample method. Low-to-high convolution is shown as (6):

$$\begin{aligned} &Y_H^{LH} = \uparrow 2(W_{LH} * X_L) \\ &shape(B, T, F, filters) \end{aligned} \tag{6}$$

Where W_{LH} is the convolutional weight matrix for the low-to-high frequency path, the shape of Y_H^{LH} is (B, T, F, filters). The sign $\uparrow$ also denotes the up-sample method. Low-to-low convolution is also shown as (7):

$$\begin{aligned} &Y_L^{LL} = W_{LL} * X_L \\ &shape(B, \frac{T}{2}, \frac{F}{2}, filters) \end{aligned} \tag{7}$$

Where W_{LL} is the convolutional weight matrix for the low-to-low frequency path, the resulting Y_L^{LL} has the shape (B, T/2, F/2, filters). The outputs from the convolutions are combined to form the high-frequency and low-frequency feature maps. This combination is performed as follows. High-frequency feature map can be shown by (8):

$$Y_H = Y_H^{HH} + Y_H^{LH}$$
$$shape(B,T,F,filters) \tag{8}$$

Where Y_H has the shape (B, T, F, filters). Low-frequency feature map is presented in (9):

$$Y_L = Y_L^{HL} + Y_L^{LL}$$
$$shape(B,\frac{T}{2},\frac{F}{2},filters) \tag{9}$$

Where Y_L retains its shape (B, T/2, F/2, filters). The final feature map Y is obtained by combining the high-frequency and low-frequency feature maps and displayed in (10):

$$Y = Y_H + \uparrow 2(Y_L)$$
$$shape(B,T,F,filters) \tag{10}$$

Here, the up-sampling operation ensures that Y_L matches the spatial dimensions of Y_H, resulting in a final feature map Y with the shape (B, T, F, filters). Equations (9) and (10) use the up-sampling and convolution processes to integrate low-frequency data into the high-pass frequency. It decomposes inputs into high and low-frequency components, reducing computational load–especially beneficial as low-frequency components dominate battery data. This enables scalable and faster processing, critical for SoH monitoring. Additionally, octave convolution improves multi-scale feature capture by independently processing frequencies, enhancing the detection of sudden changes and long-term trends. It also minimizes feature map redundancy, producing compact and informative representations that improve model generalization and prediction accuracy. Overall, octave convolution effectively utilizes high and low-frequency features, enhancing SoH estimation accuracy and efficiency compared to traditional methods.

C. Performance metrics

The architecture of the method is divided into three main components: preprocessing, training, and estimation steps, as depicted in Fig. 1. During preprocessing, battery-related data such as voltage, current, temperature, and capacity are normalized using (11):

$$z_i^k = \frac{X_i^k - \min(x)}{\max(x) - \min(x)} \rightarrow i \in \{1,...,n\} \tag{11}$$

Regarding (11) the set of X_i^k and n represents the number of samples for each cycle; given that x is a set of all charge cycles. Following the estimation, a de-normalization procedure is applied to the data. The required data is split into three sections in the following step: train set, validation set, and test set. Batteries 5, 6, and 7 were utilized for training, and battery number 18 was used to determine the SOH. The data has been normalized and is ready to be fed into the network. The extracted battery features from the dataset–such as voltage, current, and temperature during discharge–are fed into the network as input data during the training phase. The Octave convolutional and LSTM layers were used together. The proposed method estimates the SOH of batteries by significantly reducing network parameters and increasing training speed. To enhance performance, the network integrates Octave Convolution with LSTM, forming the Octave+LSTM network. Finally, the model is tested and outcomes are compared with other methods in this field. The results will be thoroughly analyzed.

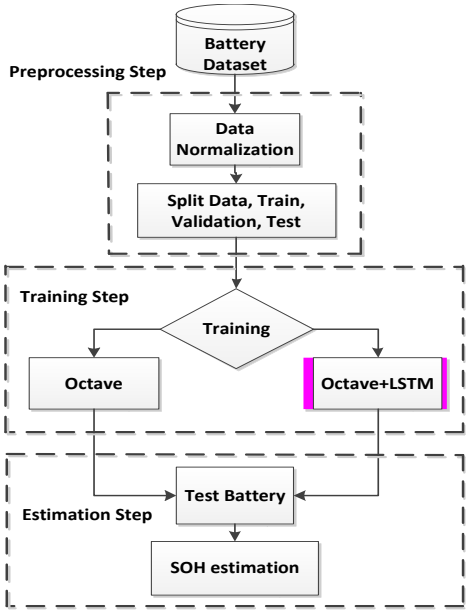

Fig. 1. Block diagram of the OCT-LSTM proposed method.

III. Experiment Data

A. Battery dataset

This section evaluates several parameters, including voltage, current, capacity, impedance, and temperature for SOH estimation by examining features of the NASA Li-ion battery dataset. It is important to note that the Prognostics Center of Excellence (PCoE) gathered and made available this dataset. The Li-Cobalt type LG Chem 18650 2.1Ah and 4.2V batteries were produced by Idaho National Laboratory [24]. Table I provides the features of batteries. Additional information about this dataset can be found in [25]. The batteries that were used for testing have the following labels: B0005, B0006, B0007, and B0018. The charging and discharging were carried out at room temperature 24°C. The charging process was conducted in Constant Current (CC) mode at 1.5A until the battery voltage attained 4.2V. The charging current was then reduced to 20mA in the Constant Voltage (CV) mode. The batteries B0005, B0006, B0007, and B0018 were discharged at a constant current of 2A until their voltages dropped to 2.7V, 2.5V, 2.2V, and 2.5V, respectively. Table II provides an overview of the experimental tests of the batteries. The lifetime of the battery

TABLE I. TEST CONDITION OF NASA DATASET [25]

Battery number	Condition			
	Voltage upper limit (V)	*Voltage lower limit (V)*	*Discharge current (A)*	*Rated capacity (Ah)*
No.5	4.2	2.7	2	2
No.6	4.2	2.5	2	2
No.7	4.2	2.2	2	2
No.18	4.2	2.5	2	2

TABLE II . BATTERIES SPECIFICATIONS

Battery Properties	18650 LIBs
Manufacture	LG Chem
Chemistry	18650 lithium cobalt oxide
Nominal capacity	2.1 Ah
Voltage range	3- 4.2 V

is determined by defining its capacity decrease to 70 percent of its nominal capacity (2Ah), based on dataset descriptions. SOH estimation relies on analyzing changes in parameters like capacity and internal impedance, relating to the battery capacity [26]. Fig. 2 illustrates the reduction in battery capacity during the discharge process, which is referred to as SOH and defined by (12), directly impacts and shortens the overall battery lifespan [27].

$$SOH = \frac{C_n}{C_c} \times 100 \tag{12}$$

In (12) C_n and C_c are the battery's nominal capacity and calculated capacity during each discharge cycle, respectively. Fig. 2 depicts the capacities of batteries B0005, B0006, B0007, and B0018, demonstrating battery capacity does not change uniformly with cycles. Furthermore, the SOH estimation is influenced by regenerative effects, rendering cycle counting less reliable. This slight improvement has a significant impact on capacity estimation. Thus, considering undesirable battery reactions, data-driven estimation methods provide more reliable results by accounting for these factors. According to the first discharge cycle, the initial capacity of B0005 is 1.8565Ah, decreasing to 1.2875Ah after the charge and discharge process. The capacity of battery B0006 has dropped from 2.0353mAh to the 1.1538mAh. According to reports, the values for B0007 are 1.8911mAh and 1.4005mAh, respectively. After experiments, the maximum value among the initial ones, 1.8550mAh, belonged to B0018 and was lowered to 1.3411mAh.

IV. Experimental Results and Discussion

Various network architectures, including CNN, OCT, LSTM, CNN-LSTM, and OCT-LSTM, were implemented and evaluated for the experiments. The training was conducted on Google Colab, utilizing a Linux system with 128GB memory and an NVIDIA Tesla P100 GPU with 16GB memory. MSE was employed as the loss function, and the Adam optimizer was used with a learning rate of 0.001. The training consisted of 500 steps with a batch size of 50, and ReLU was used as the activation function. Models performance was assessed using MSE, RMSE, and MAE error functions as per (13), (14), and (15), respectively. In this case, (13) demonstrates the calculation of MSE.

$$MSE = \frac{1}{n}\sum_{1}^{n}\left(y_i - \hat{y}_i\right)^2 \tag{13}$$

$$RMSE = \left(\frac{1}{n} \times \sum_{1}^{n}(y_i - \hat{y}_i)^2\right)^{\frac{1}{2}} \rightarrow i \in \{1,2,...,n\} \tag{14}$$

$$MAE = \frac{1}{n}\sum_{1}^{n}\left|y_i - \hat{y}_i\right| \tag{15}$$

Equations (13) and (14) outline the calculation for mean squared error and root mean squared error, which signifies the variance between the model's predicted values (y_i) and the actual values ($\hat{y}_i$). The mean absolute error is depicted by (15). In (13), (14), and (15) 'n' denotes the total number of cycles in the dataset for each battery. The parameter 'y' represents the predicted capacity of the battery in Ah, while 'ŷ' denotes the battery's actual capacity. This section presents comprehensive results from networks used for battery SOH estimation, evaluated using MSE, RMSE, and MAE. Additionally, the number of parameters utilized in the networks is fully disclosed for thorough comparison. Fig. 3 presents the outcomes of capacity estimation across various network architectures including CNN, OCT, LSTM, CNN-LSTM, and OCT-LSTM. Notably, the OCT-LSTM network demonstrates maximum accuracy in estimation, whereas CNN and OCT networks exhibit heightened fluctuations. It was observed that the LSTM network performed better than the OCT and CNN networks. This improvement stems from LSTM's effectiveness in time-series regression tasks, and the combination of CNN and OCT achieves optimal results with this network. Fig. 3 illustrates the outcomes of the SOH of battery number 18, which has undergone 120 charge and discharge cycles. A health value of 70% is set as the failure

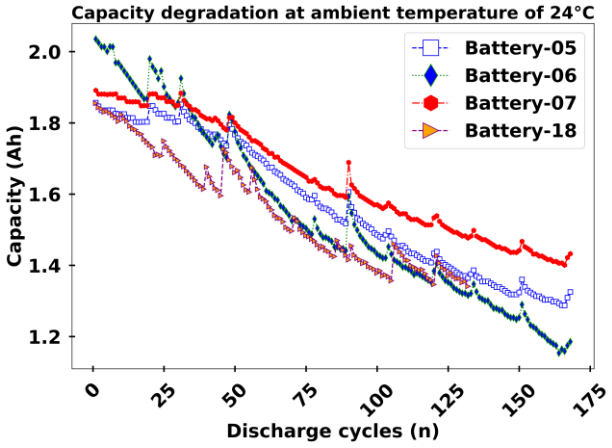

Fig. 2. Capacity chart for the batteries of dataset.

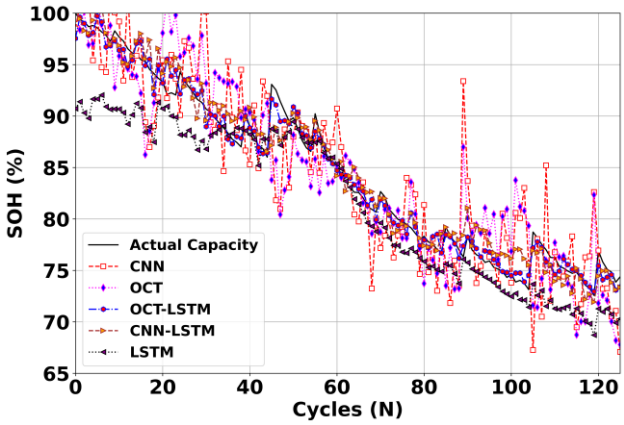

Fig. 3. Experimental results for battery 18.

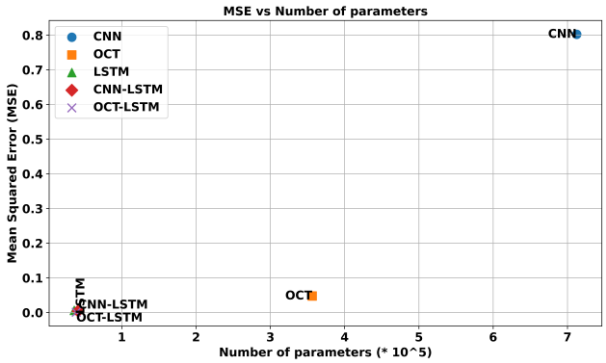

Fig. 4. Number of parameters and the mean squared error (MSE).

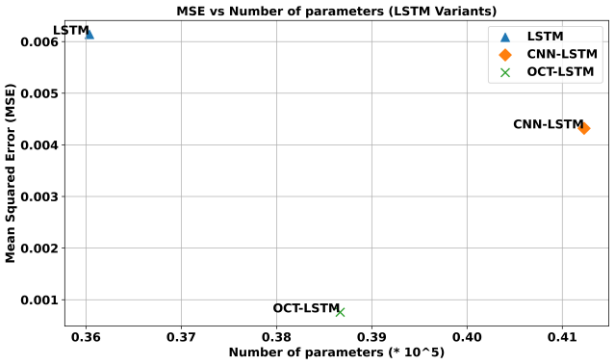

Fig. 5. Number of parameters and the MSE error for three architectures: LSTM, CNN-LSTM, and OCT-LSTM.

threshold, indicating the minimum acceptable battery health level. At the initiation of the test, the battery's health level stood at 100%, gradually declining to 70%. Notably, Fig. 3 outlines differences in battery health predictions across networks, due to battery regeneration phenomena. It also clarifies the evaluation and validation of network performance. Fig. 4 portrays the trade-off relationship between the number of parameters and the calculated error. The selection of parameter values is optimized to yield the most favorable outcome for each network. The x-axis ranges from 0 to 7 multiplied by 10^5, representing the number of parameters, while the y-axis indicates the estimated error, ranging from 0 to a maximum of 0.8. In this figure, the CNN network exhibits the poorest performance, with an error value of approximately 0.8. Conversely, the OCT network demonstrates a notable enhancement, with an error rate of 0.04 in the next place, signifying its superiority over the CNN network.

A detailed examination of the challenging networks LSTM, CNN-LSTM, and OCT-LSTM is provided in Fig. 5. The parameter values for these networks are precisely displayed, ranging from 0 to 0.41. The error values on the y-axis are presented with high precision, ranging from 0.001 to 0.006. These models exhibit a higher number of parameters compared to the LSTM network, resulting in improved performance. However, the CNN-LSTM network performs less than the LSTM network. Significantly, the OCT-LSTM network achieves the lowest estimation error, highlighting the success of this advancement. The battery capacity estimation process was commenced by examining voltage, current, and battery temperature, throughout the discharge process. Ten samples were uniformly selected for each cycle. The battery capacity estimation process is depicted in Fig. 3, wherein the CNN network exhibited the lowest performance relative to other implemented networks. The outcomes of all experiments are comprehensively presented in Table III. The

TABLE III. RESULTS OF THE EXPERIMENTS

Algorithm	**PARAMETERS**			
	MSE (%)	***RMSE (%)***	***MAE (%)***	***Number of parameters***
CNN	80.21	89.56	75.47	712524
OCT	4.74	21.772	17.872	356364
LSTM	0.614	7.837	6.085	36036
CNN-LSTM	0.4319	6.57	5.547	41228
OCT-LSTM	0.0758	2.75	1.946	38668

suggested methodology is contrasted with the current studies in this area in Table IV. A comparative examination between the CNN and OCT networks reveals a significant difference in error rates. Subsequently, the LSTM, CNN-LSTM, and OCT-LSTM networks were provided with historical data of the datasets. Evaluation of the performance metrics of these networks demonstrates that the OCT-LSTM network achieves the lowest reported error rate among other implemented networks. Furthermore, the OCT-LSTM network maintains a notably reduced parameter count compared to the CNN-LSTM network. Despite the LSTM network exhibiting fewer parameters than the CNN-LSTM and OCT-LSTM networks; it records a higher error rate. The OCT-LSTM network appeared as the top performer, achieving the lowest error rate while utilizing fewer parameters than the CNN-LSTM network, which ranked as the second-best model.

The analysis of the data presented in Table III reveals notable performance differences across the CNN-LSTM, LSTM, and OCT-LSTM networks. The CNN-LSTM network demonstrates an approximate 30% enhancement in the MSE and a 16% improvement in the RMSE compared to the LSTM network. Conversely, the OCT-LSTM exhibits the most promising practical outcome, which shows approximately 82.44% improvement in MSE and around 58.14% improvement in RMSE relative to the CNN-LSTM. Additionally, there is a substantial development in the parameter count of the OCT-LSTM compared to the CNN-LSTM. Specifically, the OCT-LSTM network achieves 87.65% improvement in the MSE and around 68.01% enhancement in the RMSE compared to the LSTM. In Table IV since the RMSE of the proposed method is the lowest value among all other papers, it represents the uniqueness of our work and serves as a remarkable milestone for this paper. Conversely, the CNN and LSTM networks fail to achieve results as effectively as the proposed OCT-LSTM network. Therefore, the OCT-LSTM method exhibits a reduction in RMSE values, higher speed, and smaller errors than

TABLE IV. OUTCOME OF THE PROPOSED METHOD COMPARED TO THE OTHER STUDIES

Methods	**X. Zhang et al.** [18]	**Z. Bao et al.** [16]	**L. Zhang et al.** [17]	**S. Amir et al.** [20]	**Proposed Method**
Procedure	GWO-BP	CNN-BiGRU	RNN	LSTM	**OCT-LSTM**
RMSE (%)	3.44	3.21	5.783	3.85	**2.75**

alternative methods. This confirms the stability and enhanced accuracy of the proposed OCT-LSTM methodology as the state-of-the-art technique in predicting the SOH.

V. Conclusion

Lithium batteries have recently become a leading area of scientific research. As a result, this paper is dedicated to exploring and contributing to this rapidly evolving field. This research introduces a novel network, described as OCT-LSTM, for lithium battery SOH estimation. The network integrates Octave Convolution and LSTM architectures with multi-input data to significantly enhance estimation accuracy. Several networks, including CNN, OCT, LSTM, and CNN-LSTM, were initially implemented for comparative analysis with the proposed network. These networks were evaluated based on the number of parameters, error metrics, and battery capacity variations per cycle. The proposed OCT-LSTM, representing a state-of-the-art approach, demonstrated significant advancements over the alternative methodologies evaluated in this study. The proposed network achieved substantial improvements, reducing MSE by 82.44% and 87.65% compared to the CNN-LSTM and LSTM networks, respectively. Moreover, the OCT-LSTM network exhibited significant enhancements in RMSE, with reductions of 58.14% and 68.01% compared to the CNN-LSTM and LSTM networks, respectively. The efficacy of this approach was validated using the NASA battery dataset. Furthermore, in cases with limited input data, data augmentation can be employed to reduce prediction errors, offering particular advantages for scenarios involving short charging intervals. Future work could implement the proposed network, trained on battery dataset, onto embedded hardware such as a Raspberry Pi for real-time SOH estimation. The empirical results demonstrate the superior accuracy of the proposed method in predicting the collective SOH of lithium-ion batteries compared to CNN, OCT, LSTM, and CNN-LSTM methodologies.

Code Availability

Code for the modeling and dataset of the batteries are available at github.com/seyed-mohammadreza-mousavi/SOH-estimation and github.com/Amirhossein-Rahimian-Zarif/NASA_Lithium_Battery_Dataset.

References

[1] K. Song, D. Hu, Y. Tong, and X. Yue, "Remaining life prediction of lithium-ion batteries based on health management: A review," *J. Energy Storage*, vol. 57, p. 106193, 2023.

[2] P. Thakkar, S. Khatri, D. Dobariya, D. Patel, B. Dey, and A. K. Singh, "Advances in materials and machine learning techniques for energy storage devices: A comprehensive review," *J. Energy Storage*, vol. 81, p. 110452, 2024.

[3] C. Lin, J. Xu, and X. Mei, "Improving state-of-health estimation for lithium-ion batteries via unlabeled charging data," *Energy Storage Mater.*, vol. 54, pp. 85–97, 2023.

[4] B. P. Adedeji and G. Kabir, "A feedforward deep neural network for predicting the state-of-charge of lithium-ion battery in electric vehicles," *Decis. Anal. J.*, vol. 8, p. 100255, 2023.

[5] A. R. Zarif, A. Kazemi, and Y. Mafinejad, "A Novel Li-Ion Battery Charge Management System for Applying in Renewable Energies Based on Pulse Charge Method," in *2024 9th International Conference on Technology and Energy Management (ICTEM)*, 2024, pp. 1–6, doi: 10.1109/ICTEM60690.2024.10631901.

[6] Z. Chen, H. Zhao, Y. Zhang, S. Shen, J. Shen, and Y. Liu, "State of health estimation for lithium-ion batteries based on temperature prediction and gated recurrent unit neural network," *J. Power Sources*, vol. 521, p. 230892, 2022.

[7] J. Zhou, S. Wang, W. Cao, Y. Xie, and C. Fernandez, "State of health prediction of lithium-ion batteries based on SSA optimized hybrid neural network model," *Electrochim. Acta*, vol. 487, p. 144146, 2024.

[8] Y. Zou, Z. Lin, D. Li, and Z. Liu, "Advancements in Artificial Neural Networks for health management of energy storage lithium-ion batteries: A comprehensive review," *J. Energy Storage*, vol. 73, p. 109069, 2023, doi: https://doi.org/10.1016/j.est.2023.109069.

[9] C. Qian *et al.*, "Convolutional neural network based capacity estimation using random segments of the charging curves for lithium-ion batteries," *Energy*, vol. 227, p. 120333, 2021.

[10] M. Lin, C. Yan, W. Wang, G. Dong, J. Meng, and J. Wu, "A data-driven approach for estimating state-of-health of lithium-ion batteries considering internal resistance," *Energy*, vol. 277, p. 127675, 2023.

[11] S. Khaleghi *et al.*, "Developing an online data-driven approach for prognostics and health management of lithium-ion batteries," *Appl. Energy*, vol. 308, p. 118348, 2022.

[12] A. Tiane, C. Okar, M. Alzayed, and H. Chaoui, "Comparing Hybrid Approaches of Deep Learning for Remaining Useful Life Prognostic of Lithium-ion Batteries," *IEEE Access*, 2024.

[13] M. Moradi and J. Hamidzadeh, "A domain adaptation method by incorporating belief function in twin quarter-sphere SVM," *Knowl. Inf. Syst.*, vol. 65, no. 7, pp. 3125–3163, 2023.

[14] A. P. Renold and N. S. Kathayat, "Comprehensive Review of Machine Learning, Deep Learning, and Digital Twin Data-Driven Approaches in Battery Health Prediction of Electric Vehicles," *IEEE Access*, vol. 12, pp. 43984–43999, 2024.

[15] P. Yang *et al.*, "Joint evaluation and prediction of SOH and RUL for lithium batteries based on a GBLS booster multi-task model," *J. Energy Storage*, vol. 75, p. 109741, 2024.

[16] Z. Bao, J. Jiang, C. Zhu, and M. Gao, "A New Hybrid Neural Network Method for State-of-Health Estimation of Lithium-Ion Battery," *Energies*, vol. 15, no. 12, pp. 1–16, 2022.

[17] L. Zhang, T. Ji, S. Yu, and G. Liu, "Accurate Prediction Approach of SOH for Lithium-Ion Batteries Based on LSTM Method," *Batteries*, vol. 9, no. 3, 2023, doi: 10.3390/batteries9030177.

[18] X. Zhang, J. Hou, Z. Wang, and Y. Jiang, "Joint SOH-SOC estimation model for lithium-ion batteries based on GWO-BP neural network," *Energies*, vol. 16, no. 1, p. 132, 2022.

[19] H.-L. Feng and A.-K. Xu, "A Data Compensation Model for Predicting SOH and RUL of Lithium–Ion Battery," *J. Electr. Eng. Technol.*, vol. 19, no. 1, pp. 395–406, 2024.

[20] S. Amir, M. Gulzar, M. O. Tarar, I. H. Naqvi, and N. A. Zaffar, "Dynamic Equivalent Circuit Model to Estimate State-of-Health of Lithium-Ion Batteries," *IEEE Access*, vol. 10, pp. 18279–18288, 2022, doi: 10.1109/ACCESS.2022.3148528.

[21] M. Haghighi, M. R. Masoudi, and M. Rahimipour Behbahani, "Smart Homes Energy Management System Integrated with Renewable Energy Sources and Demand Response Programs," *Power, Control. Data Process. Syst.*, vol. 2, no. 1, 2025.

[22] M. R. Masoudi, M. Haghighi, and M. Rahimipour Behbahani, "Optimal Operation of Solar Energy System integrated with Energy Storage Systems," *Power, Control. Data Process. Syst.*, vol. 1, no. 1, 2024.

[23] M. Monemi Bidgoli and R. Ghani, "Optimal Energy Management of Water-Energy Nexus in Multi-Carrier Systems Integrated with Renewable Sources," *Power, Control. Data Process. Syst.*, vol. 1, no. 1, 2024.

[24] B. Saha and K. Goebel, "Uncertainty management for diagnostics and prognostics of batteries using Bayesian techniques," in *2008 IEEE aerospace conference*, 2008, pp. 1–8.

[25] B. Bole, C. Kulkarni, and M. Daigle, "Randomized battery usage data set," *NASA AMES Progn. data Repos.*, vol. 70, 2014.

[26] W. Liu, Y. Xu, and X. Feng, "A hierarchical and flexible data-driven method for online state-of-health estimation of Li-ion battery," *IEEE Trans. Veh. Technol.*, vol. 69, no. 12, pp. 14739–14748, 2020.

[27] H. Sun, J. Sun, K. Zhao, L. Wang, and K. Wang, "Data-driven ICA-Bi-LSTM-combined lithium battery SOH estimation," *Math. Probl. Eng.*, vol. 2022, pp. 1–8, 2022.